RSC Advances



PAPER

View Article Online
View Journal | View Issue



Cite this: RSC Adv., 2023, 13, 27782

Perovskite SrZrO₃:Ho³⁺ phosphors: synthesis, structure, Judd-Ofelt analysis and photoluminescence properties

Vijay Singh (10 ** and M. Seshadri b

A series of $SrZrO_3:xHo^{3+}$ (x=0.01, 0.03, 0.05, 0.07, 0.09, and 0.11 mol) perovskite phosphors have been synthesized by using the sol-gel technique. The structural and optical characteristics of the prepared phosphors have been investigated through powder XRD, FT-IR, UV-visible diffuse reflectance, and photoluminescence analysis. The photoluminescence emission spectra showed a bright characteristic peak at 545 nm (5F_4 + 5S_2 \rightarrow 5I_8) under the 454 nm excitation, which exhibits emission in the green region of the electromagnetic spectrum. The emission intensity of the phosphors starts decreasing slowly beyond 3 mol% Ho^{3+} ions concentration due to concentration quenching, which is attributed to the dipole–dipole interaction between Ho^{3+} ions. The site symmetry of the Ho^{3+} ions has been studied by estimating the relative Judd–Ofelt intensity parameters (Ω_{λ} , where $\lambda=2$, 4, 6) from the photoluminescence excitation spectrum of the $SrZrO_3:0.03Ho^{3+}$ phosphor. The obtained findings suggest that the synthesized phosphors will be favorable for their bright green emission and thus, can be widely used for different optoelectronic applications.

Received 21st June 2023 Accepted 7th September 2023

DOI: 10.1039/d3ra04175a

rsc.li/rsc-advances

1. Introduction

Perovskite materials with the general formula ABO₃ (where A = Ca, Sr, Ba; and B = Zr, Hf, Ti) have great versatility and outstanding chemical, physical, electrical, and thermomechanical properties. These host lattices are getting special attention due to their potential applications as catalysts, photocatalysts, fuel cells, in photovoltaic applications, optoelectronics, and solid oxide fuel cells.1-3 Perovskite materials possess a fascinating feature in which a slight variation in structure and chemical composition may result in enormous changes in their chemical and physical properties.4-7 The doping of a foreign element into these ABO3 type inorganic oxides influences their optical and magnetic properties by creating various defects.8,9 Especially, lanthanide ions as dopants are suitable candidates since they exhibit unique spectroscopic properties. 10-12 The coordination geometry and oxidation states of uranium ions in the SrZrO₃ perovskite were studied by Gupta et al., 13 although Li et al.14 investigated the spectral characteristics and intrinsic defects of SrZrO3 perovskite. The earlier report published by Knight et al.15 reveals the structural and thermoelastic characteristics of SrZrO₃ perovskite.

Perovskites have been reported to be advantageous in high-temperature applications, like hydrogen gas sensors, steam

electrolysis, and fuel cells.16-18 Proton conductivity at elevated temperature enables its usage in typical electrochemical devices. Among different perovskite materials, the SrZrO₃ host material has been suggested for use as a potential substrate due to its large single crystals.19 In recent years, the structural phase transitions of strontium zirconate perovskites have been studied significantly at room temperature and higher temperatures.20-22 Initially, the structural investigations revealed that the SrZrO₃ possesses an orthorhombic phase at room temperature, and later Carlsson²³ proposed the presence of additional phases at high temperatures. Mete et al. 17 examined the structural and electronic characteristics of 4d-perovskite: the cubic phase of SrZrO3. The electronic and structural performances of selected surfaces of SrZrO3 were investigated by Sambrano et al.24 Singh et al.25 have also published research on the photoluminescence and structural properties of SrZrO₃:Sm³⁺ orange-emitting perovskite phosphors.

Due to long-lived excited states and energy levels, the trivalent lanthanide ions doped luminescent materials (using Tm^{3+} , Er^{3+} , and Ho^{3+} ions) have been selected as the main subject of interest by several research groups. ^{26–28} Holmium belongs to the lanthanides and its electronic configuration becomes [Xe]4f¹⁰ when doped into a crystalline host. Several spectroscopic studies revealed that Ho^{3+} is the most desirable ion for midinfrared lasers and has excellent green emission properties other than Tb^{3+} (green emission only) ions among the rare earth ions due to its various electronic transitions. Ranjan *et al.* ²⁹ reported the enhanced green up-conversion emission of Ho^{3+} doped Gd_2O_3 phosphor by co-doping with Yb^{3+} ions. The luminescence studies of Eu^{3+} and Ho^{3+} doped Sr_2TiO_4 revealed

^aDepartment of Chemical Engineering, Konkuk University, Seoul 05029, Republic of Korea. E-mail: vijayjiin2006@yahoo.com

^bDepartment of Physics, Koneru Lakshmaiah Education Foundation, Hyderabad 500043, Telangana, India

that the Sr₂TiO₄ could be a suitable material in favor of highpressure mercury vapor lamps or white light-emitting diodes.³⁰

A literature survey confirms a lack of reports available on Ho³⁺ doped ABO₃ type zirconate perovskites. The Ho³⁺ is often used as a structural probe because it can be accommodated at the A-place or B-place of perovskite oxides and in-site changes in the optical behavior and local site surrounding these doped oxide materials. Based on these results, our prepared sample possesses excellent thermal and chemical stability, prompting its practical application. Combining trivalent rare-earth metal ions in zirconate perovskites is considered as a promising approach to developing more useful and stable luminescent materials. Shi et al.31 prepared Yb3+, Ho3+, Li+ tri-doped TiO2 upconversion materials to enhance the efficiency of perovskite solar cells. First, Hou et al. 32 investigated the impacts of Ho³⁺ ion doping over the surface morphology, crystal phase, and magnetic characteristics of BiFeO₃ thin films synthesized by the sol-gel technique. Sharif et al.33 investigated surface morphology, structural, magnetic, and dielectric properties in

Table 1 Detailed information of sample composition and starting materials

~ 1	Weight of starting materials (g)				
Sample compositions	Sr(NO ₃) ₂	$ZrO(NO_3)_2 \cdot 2H_2O$	C ₆ H ₈ O ₇	Ho(NO ₃) ₃ ·5H ₂ O	
SrZrO ₃ :0.01Ho	0.8464	1.0688	3.0738	0.0176	
SrZrO ₃ :0.03Ho	0.8464	1.0688	3.0738	0.0592	
SrZrO ₃ :0.05Ho	0.8464	1.0688	3.0738	0.0882	
SrZrO ₃ :0.07Ho	0.8464	1.0688	3.0738	0.1243	
SrZrO ₃ :.0.09Ho	0.8464	1.0688	3.0738	0.1578	
SrZrO ₂ :0.11Ho	0.8464	1.0688	3.0738	0.1940	

the BiFeO $_3$ with holmium-doped thin films deposited by the pulsed laser deposition technique. Moreover, Hussain *et al.*³⁴ presented resistive leakage and intrinsic polarization analyses for high-performance piezo/pyroelectric Ho-doped 0.64Pb(Mg $_1$ / $_3$ Nb $_2$ / $_3$)O $_3$ -0.36PbTiO $_3$ binary ceramic materials.

Besides the solid-state reaction process, a conventional synthetic route for preparing phosphor particles, several new synthetic methods have already been developed, for example, co-precipitation, sol-gel, solution combustion, microemulsion, spray pyrolysis, and hydrothermal synthesis. The present work uses the sol-gel method to prepare SrZrO₃ phosphor. Sol-gel is a synthetic route to synthesize ceramic oxides, which provides reasonable control over stoichiometry, high purity, good homogeneity, and reduced sintering temperature. This method may also enable the production of low-temperature phases. A sol-gel method in a liquid includes a polycondensation reaction, which builds the oxide network of a molecular precursor. Although the process consists of several steps, doping concentration positively impacts the luminescence and crystal structural properties of the prepared phosphor. Wurm et al. 35 prepared sol-gel SrZrO3 and SrTiO3 coatings on C and SiCfibers. Venkatesh et al. 36 prepared a novel strontium zirconate perovskite coating on an Inconel substrate using the sol-gel synthesis method. Liu et al.37 reported sol-gel derived SrZrO3 memory thin films with resistance switching properties. In this work, the Ho³⁺ doped SrZrO₃ perovskite phosphors were synthesized by using sol-gel synthesis. The prepared phosphors were characterized structurally and optically. To know the spectral characteristics, the measured photoluminescence excitation spectra were used to calculate the Judd-Ofelt intensity parameters, Ω_2 , Ω_4 & Ω_6 . Detailed photoluminescence properties are discussed herein.

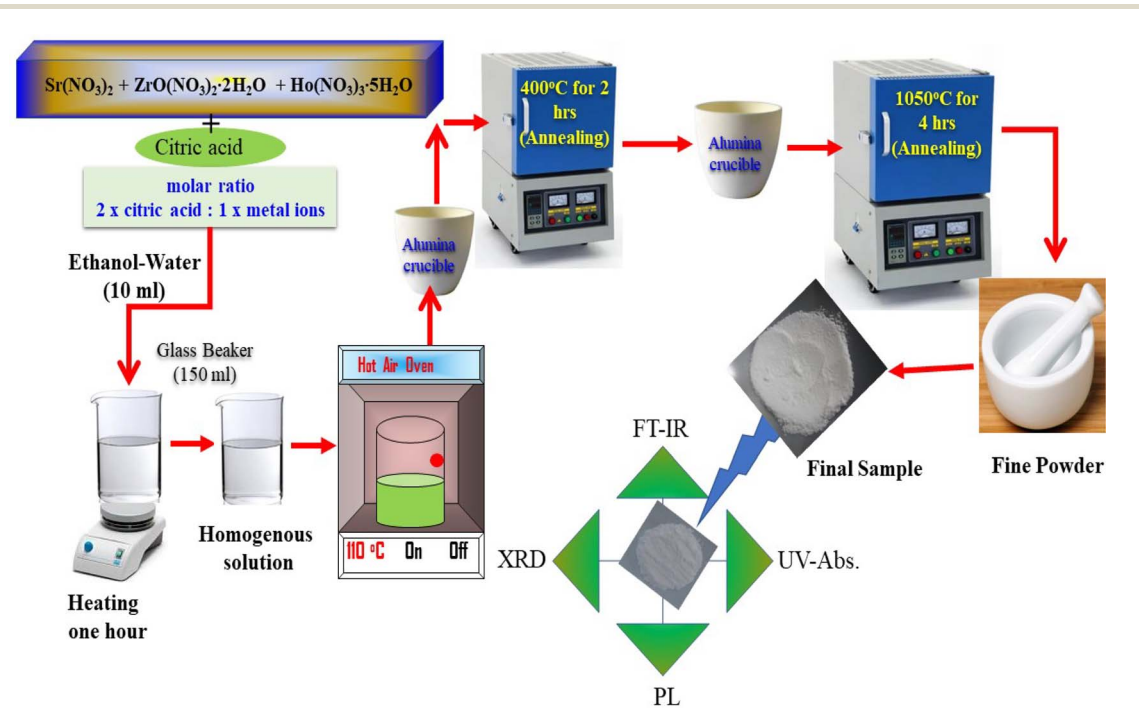


Fig. 1 Systematic diagram of synthesis process of the sample.

2. Materials preparation and analysis

The $SrZrO_3$: xHo^{3+} (x = 0.01, 0.03, 0.05, 0.07, 0.09, and 0.11 mol)perovskite phosphors were fabricated by sol-gel procedure. The quantity of the employed starting materials is reported in Table 1. As per the chemical formulae, the stoichiometric quantities of strontium nitrate (Sr(NO₃)₂) (Sigma-Aldrich, purity: 99%), zirconium nitrate oxide dihydrate (ZrO(NO₃)₂-·2H₂O) (Kanto chemical, purity: 99%), holmium(III) nitrate pentahydrate (Ho(NO₃)₃·5H₂O) (Sigma-Aldrich, purity: 99.9%), citric acid (C₆H₈O₇) (Junsei, purity: 99.5%) and, a mixture of 6 ml of ethanol and 4 ml of water combine in a 150 ml beaker. The molar ratio was kept at 2:1 according to citric acid and total metal ions. Next, the mixture was stirred for 1 h to achieve a clear homogeneous solution; after that, put the resultant in the oven until the solution dried. A hot temperature furnace maintained at 400 °C preheated the acquired gels for 2 h in air. After preheating, the samples were granulated and fired for 4 h at 1050 °C in the ambient condition, giving the fine powder samples. Fig. 1 presents a pictorial view of the synthesis process.

The X-ray diffraction patterns were monitored by a RIGAKU (Miniflex-II) diffractometer attached to an X-ray source (Cu-Kα radiation, $\lambda=1.5406$ Å); the scan rate was set at 5° per minute between 10° –80° for 2 θ angle. To identify the functional group present in the prepared samples, a Fourier transform infrared (6700, Thermo Fisher Nicolet) spectrometer was operated in a range of 400–4000 cm $^{-1}$. A small quantity of prepared SrZrO $_3$:Ho $^{3+}$ phosphor powder is used to measure diffuse reflectance with A Cary-5000 (UV-VIS-NIR) spectrophotometer coupled to a Praying Mantis diffuse reflectance accessory. Photoluminescence (PL) spectra were analyzed by a Shimadzu (RF-5301PC) spectrofluorophotometer fitted with a Xenon-flash lamp. The emission and excitation spectra were recorded using a spectral slit width of 1.5 nm. The above characterizations were performed at room temperature.

Results and discussion

3.1 Crystal structure

The XRD measurement was conducted to study the structural phase and crystallinity of the prepared samples. Fig. 2 displays the XRD patterns of the SrZrO3:xHo3+ powders. For the synthesized phosphors, the major diffraction peaks matched with JCPDS (Joint Committee for Powder Diffraction Standards Card) File No. 76-0167 corresponding to SrZrO₃. The effect of Ho^{3+} ions (at the studied concentrations *i.e.* 0.01, 0.03, 0.05, 0.07, 0.09, and 0.11 mol) on the structure of the SrZrO₃ lattice seems to be negligible as XRD patterns remain the almost same at different doping concentrations. However, we believe the actual doping level can be clarified by Le Bail method to find the evolution trend of the cell lattice parameters. To calculate the crystalline size, the FWHM (full width at half maximum) of dominant (110) diffraction peaks are considered in leading Scherrer's equation, $D = 0.9\lambda/\beta \cos \theta$, in which the wavelength of incident X-rays is denoted as λ , the corresponding Bragg's diffraction angle is θ , and the FWHM of the (110) peak is β . The

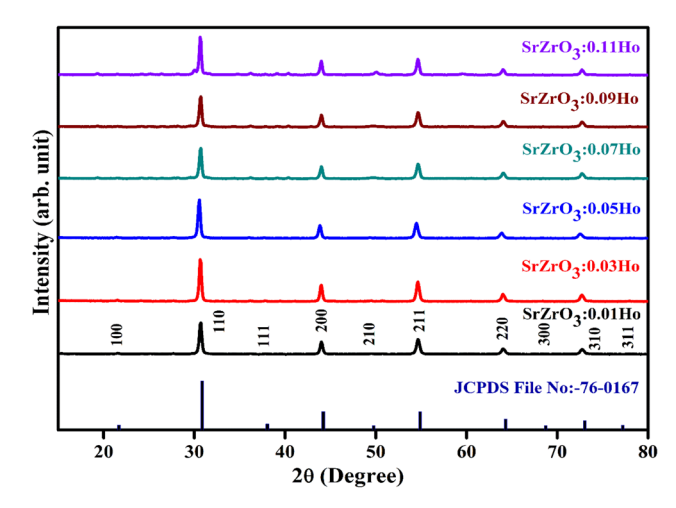


Fig. 2 Powder XRD patterns of SrZrO₃:xHo³⁺ phosphors

determined crystal sizes were approximately within the range of 24–31 nm. Various oxides with the ABO $_3$ chemical formula follow the perovskite structure. Fig. 3 showed the simplified crystal lattice of the SrZrO $_3$ perovskite. The SrZrO $_3$ has cubic symmetry with a $Pm\bar{3}m[221]$ space group. In the SrZrO $_3$ perovskite structure, the Sr atoms are situated on the edges of the cubic unit cell, and the 12 closest neighbor O atoms surround the Sr atoms. Similarly, the Zr atom is situated in the centrum of the unit cell and is six-fold integrated with the O closedneighbor atoms, making an octahedron. The cubic unit cell faces have O atoms, which are two-fold coordinated with Zr neighbor atoms. The Zr-ion and Sr-ion have the coordination numbers 6 and 8, respectively. 1,11

3.2 Vibrational analysis

Fig. 4 shows a typical vibrational feature of the SrZrO₃:0.03Ho³⁺ powder sample. An intense absorption band at 558 cm⁻¹ is attributed to the Zr–O stretching vibration. We have also observed a sharp peak at 857 cm⁻¹. Katyayan and Agrawal⁸ studied SrZrO₃:Eu³⁺, Tb³⁺ system and several peaks reported in the range of 509–895 cm⁻¹ were due to the vibrational stretching modes of metal–oxygen bond, *i.e.*, Zr–O bond. However, few peaks lie between 1000 and 1270 cm⁻¹ due to the active modes of asymmetric stretching of impurity ions. Further, sharp peaks were reported within 1302–1588 cm⁻¹ due to the symmetrical stretching of Sr–O bonds. We have also observed bands at 1018 and 1458 cm⁻¹. The observed bands and their assignments can be confirmed with the previous literature.^{8,38–41}

3.3 Diffuse reflectance spectra and optical band gap

The UV-diffuse reflectance spectra were recorded between the wavelength regions of 200–800 nm for the 3 mol% $\mathrm{Ho^{3^+}}$ doped $\mathrm{SrZrO_3}$ phosphor. Fig. 5 shows the diffuse reflectance spectrum and extracted absorption coefficient with the Kubelka–Munk function. It can be seen that few bands around 365, 421, 454, 468, 489, 542, and 645 nm are related to the 4f–4f configuration of $\mathrm{Ho^{3^+}}$ transitions: ${}^5\mathrm{I_8} \rightarrow {}^5\mathrm{G_5}, {}^4\mathrm{I_8} \rightarrow {}^5\mathrm{G_5}, {}^5\mathrm{I_8} \rightarrow {}^5\mathrm{G_5}, {}^5\mathrm{I_8}, {}^5\mathrm{G_5}, {}^5\mathrm{I_8} \rightarrow {}^5\mathrm{G_5}, {}^5\mathrm{I_8} \rightarrow {}^5\mathrm{G_5}, {}^5\mathrm{I_8}, {}^5\mathrm{G_5}, {}^5\mathrm{I_8} \rightarrow {}^5\mathrm{G_5}, {}^5\mathrm{I_8}, {}^$

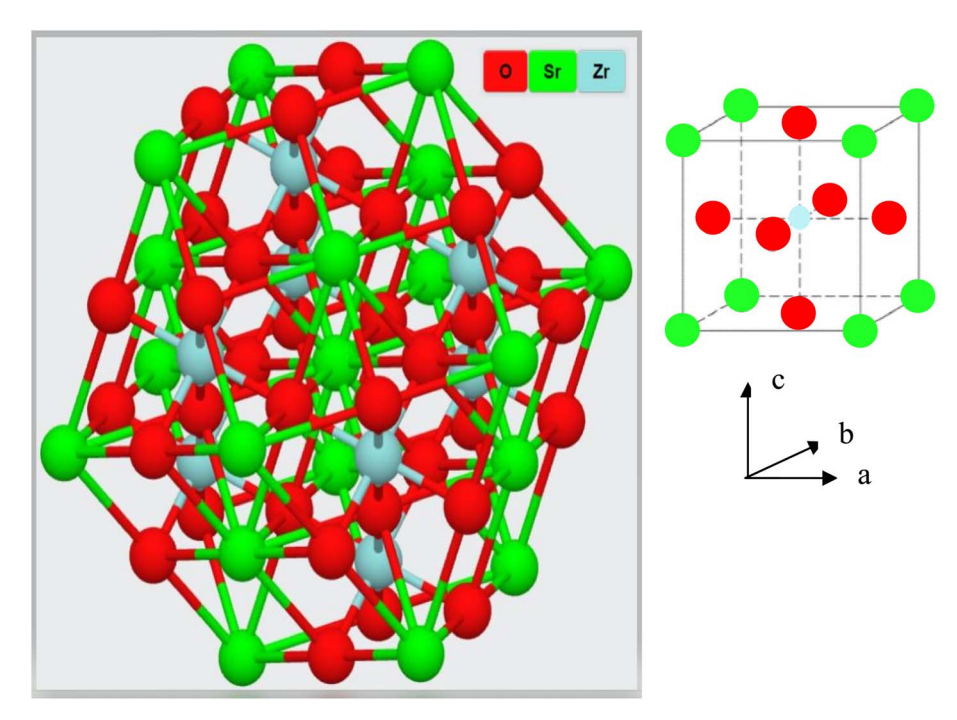


Fig. 3 Crystal structure of the SrZrO₃ perovskite.

 5F_1 , $^5I_8 \rightarrow ^5F_2 + ^3K_8$, and $^5I_8 \rightarrow ^5F_3$, respectively. The extracted optical-absorption coefficient (α cm $^{-1}$) was calculated by the consecutive expression:⁴²

$$F(R) = \frac{\left(1 - R\right)^2}{2R} = \alpha \tag{1}$$

where R stands for sample reflectance. The $E_{\rm g}$ (optical band gaps) for the ${\rm Ho^{3^+}}$ doped ${\rm SrZrO_3}$ phosphor can be estimated with the Tauc relation:⁴³

$$F(R)\hbar\omega \approx A(\hbar\omega - E_{\rm g})^n \tag{2}$$

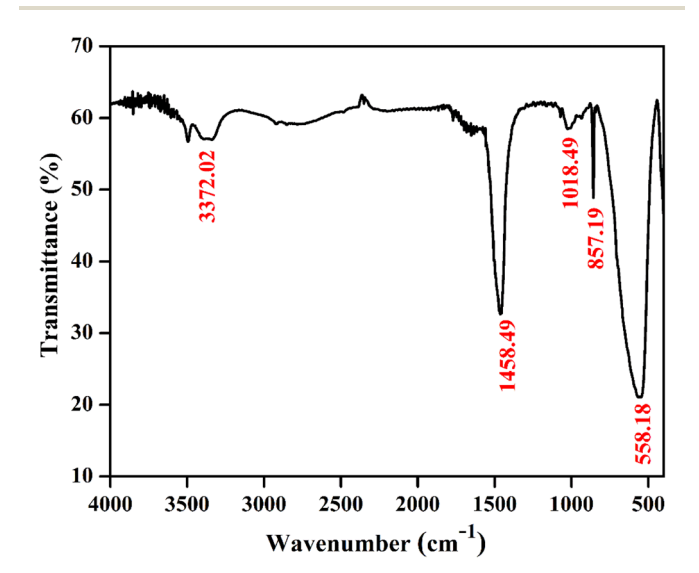


Fig. 4 FTIR spectrum of SrZrO₃:0.03Ho³⁺ phosphor.

where A is a constant, F(R) is the absorption coefficient with photon energy $(\hbar\omega)$ and n represents the power factor: n=1/2 allowed direct transitions, and n=2 allowed an indirect transition. Fig. 6 shows plots of $(F(R)\hbar\omega)^n$ as a function of $\hbar\omega$ (eV). After assuming $(F(R)\hbar\omega)^2=0$ and $(F(R)\hbar\omega)^{1/2}=0$ for the linear region within the plot, the energy band gaps of the direct allowed and indirectly allowed transitions were observed to be 5.21 eV and 5.43 eV, correspondingly for the SrZrO₃:0.03Ho³⁺ phosphor.

3.4 Photoluminescence analysis

Fig. 7(a) demonstrates the photoluminescence excitation (PLE) spectra for the produced Ho³⁺ doped SrZrO₃ phosphors. The

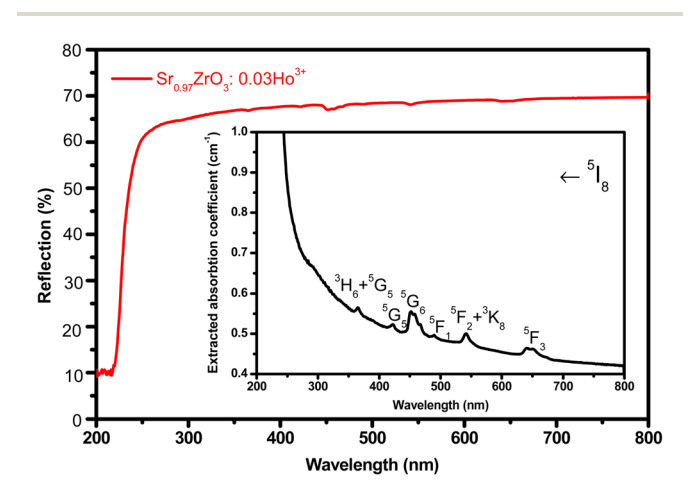


Fig. 5 UV-visible diffuse reflectance spectrum of $\rm SrZrO_3:0.03Ho^{3+}$ phosphor. Inset of the figure shows extracted absorption spectrum.

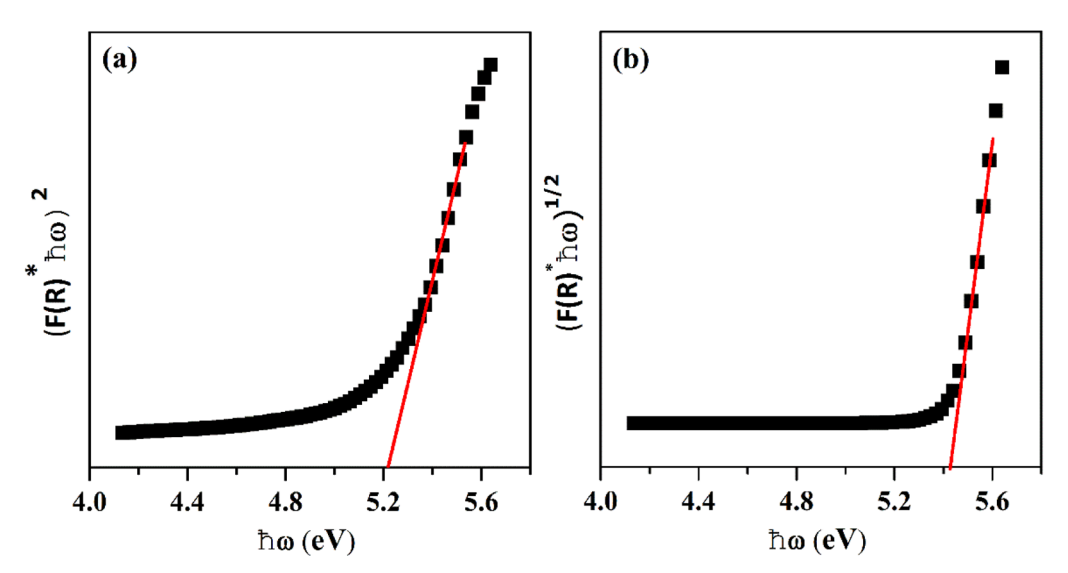
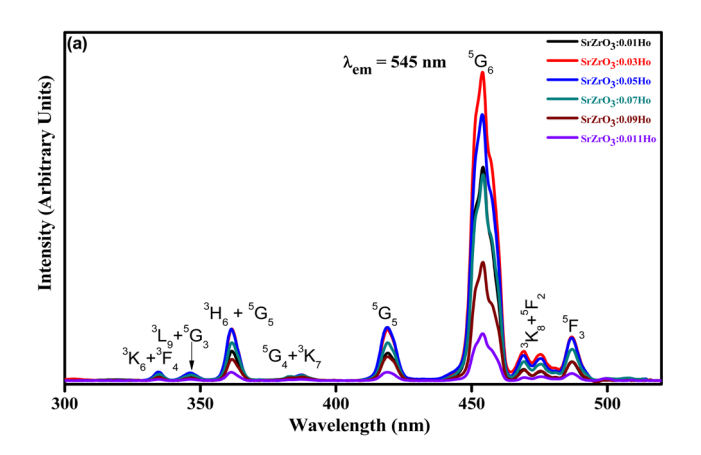


Fig. 6 Plots of $(F(R)\hbar\omega)^n$ versus $\hbar\omega$ (eV): (a) direct allowed transition and (b) indirect allowed transition.



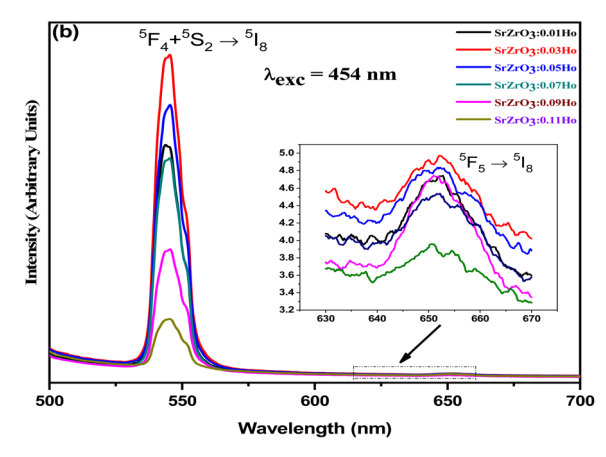


Fig. 7 (a) Photoluminescence excitation spectra of SrZrO $_3$:xHo $^{3+}$ phosphors ($\lambda_{em}=545\,$ nm) and (b) photoluminescence emission spectra of SrZrO $_3$:xHo $^{3+}$ phosphors ($\lambda_{exc}=454\,$ nm).

PLE spectra were acquired using the emission band at 545 nm. It can be read that the narrow bands owing to the 4f–4f transitions of ${\rm Ho^{3+}}$ ions and originated from ${}^5{\rm I_8}$ to ${}^3{\rm K_6} + {}^3{\rm F_4}$ (334 nm), ${}^3{\rm L_9} + {}^5{\rm G_3}$ (346 nm), ${}^3{\rm H_6} + {}^5{\rm G_5}$ (361 nm), ${}^3{\rm K_7} + {}^5{\rm G_4}$ (387 nm), ${}^5{\rm G_5}$

(418 nm), 5G_6 (454 nm), ${}^5F_2 + {}^3K_8$ (472 nm) and 5F_3 (486 nm). The highest PLE intensity was observed at 454 nm; this would be suitable as the excitation wavelength for all prepared phosphors. The PLE band intensity is saturated at 3 mol% of ${\rm Ho}^{3+}$ ions in the SrZrO $_3$ phosphor. Usually, the doping of ${\rm Ho}^{3+}$ ions in place of ${\rm Sr}^{2+}$ ions will create positive charge defects that would negatively affect luminescence. Therefore, the expected emission intensity is maximum for 3 mol% of ${\rm Ho}^{3+}$ ions, and then the subsequent decrease of emission intensity is due to the ${\rm Ho}_{\rm Sr}^{+}$ defects. 44

The emission spectra were monitored using 454 nm as the excitation wavelength for all phosphors and are presented in

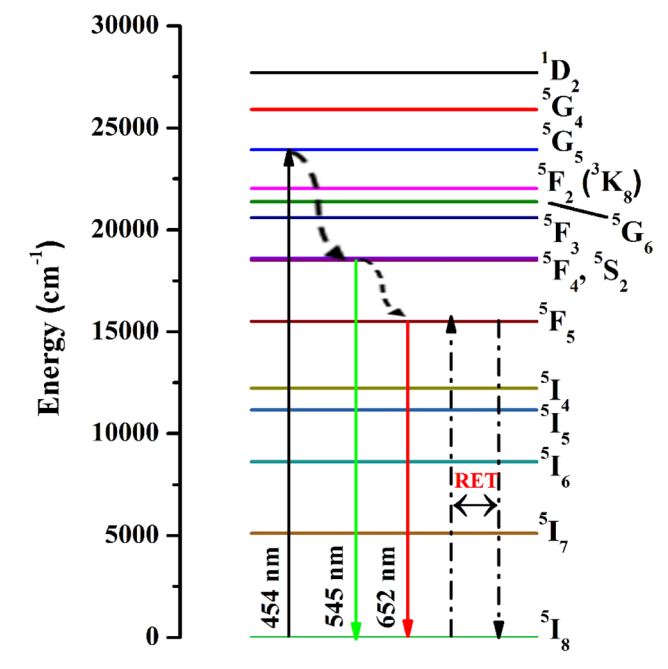


Fig. 8 Schematic energy level diagram for Ho³⁺ ions with possible radiative and non-radiative transitions.

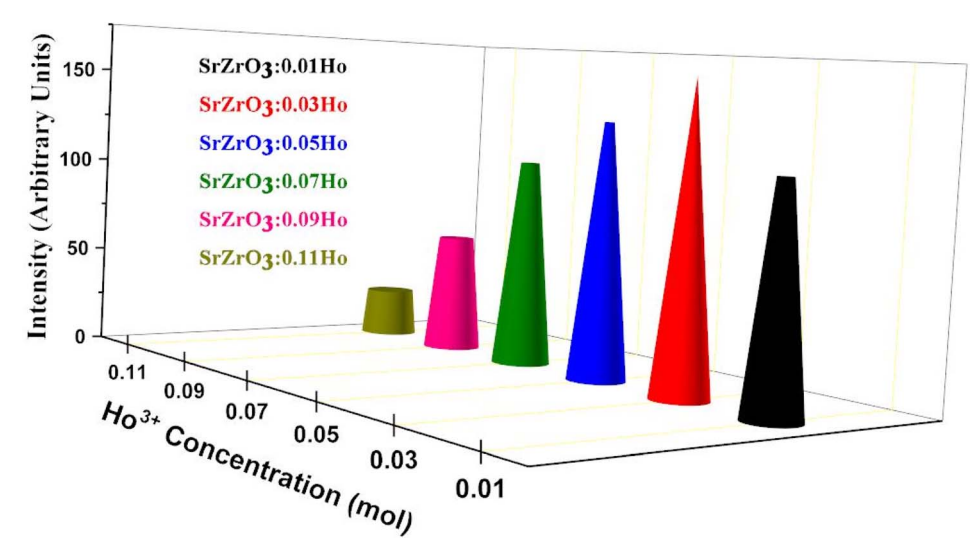


Fig. 9 Variation of emission intensity ($l_{545 \text{ nm}}$) as a function of Ho³⁺ ions in the SrZrO₃:Ho³⁺ phosphor.

Fig. 7(b). Strong green and weak red emission bands have been seen around 545 nm and 652 nm. The obtained bands are possibly defined as transitions of $\mathrm{Ho^{3+}}$ ions for ${}^{5}\mathrm{F_{4}}$ + ${}^{5}\mathrm{S_{2}}$ \rightarrow ${}^{5}\mathrm{I_{8}}$ and ${}^{5}F_{5} \rightarrow {}^{5}I_{8}$, respectively. The intensity of green emission at 545 nm is \sim 35 times more substantial than the red emission at 652 nm. Upon excitation of 454 nm, the ions are excited from ⁵I₈ to ${}^5\mathrm{G}_4$, then most of the excited ions decay the lower levels ${}^5\mathrm{F}_4$ + ⁵S₂ and ⁵F₅ levels non-radiatively, and subsequently, radiatively transit to 5I_8 level with emission of green (${}^5F_4 + {}^5S_2 \rightarrow {}^5I_8$) and red (${}^{5}F_{5} \rightarrow {}^{5}I_{8}$), respectively. The energy gap difference for the ⁵F₄ and ⁵F₅ to the next lower levels are around 3400 cm⁻¹ and 2400 cm⁻¹, thus the observed difference of green and red emission intensities depends on the population of excited states and multiphonon relaxation rates (W_{mpr}) since the W_{mpr} is increasing with the decrease of the energy gap between excited state to the next lower state. Fig. 8 shows a schematic energy level diagram for Ho³⁺ ions with possible radiative and non-radiative relaxation processes.

As seen in Fig. 9, the highest emission intensity was noticed when the $\mathrm{Ho^{3^+}}$ ions concentration was 3 mol%, and it was decreased according to the increasing concentration of $\mathrm{Ho^{3^+}}$ ions in the $\mathrm{SrZrO_3}$ phosphor because of concentration quenching. Generally, it is recognized that the Ho–Ho distance reduces with an enhancement of $\mathrm{Ho^{3^+}}$ ion concentration, leading to fluorescence quenching that comes from an increase in the resonant transfer probability between $\mathrm{Ho^{3^+}}$ ions. The chances of energy transmission distance between Ho–Ho ions are termed the critical distance ($R_{\rm c}$) obtained by the Blasse expression:

$$R_{\rm c} \approx 2 \left[\frac{3V}{4\pi \chi_{\rm c} N} \right]^{1/3} \tag{3}$$

where V is the unit cell volume, critical ion concentration is χ_c and N is the number of Zr ions of a unit cell. For our Ho³⁺ doped SrZrO₃ phosphor, V = 552.175 (Å)³,⁴⁶ N = 4, and $\chi_c = 0.03$. The calculated critical transfer distance (R_c) is ~20 Å, far greater than 5 Å that favors exchange interaction; thus, it can be

established that the observed concentration quenching in Ho³⁺ doped SrZrO₃ samples is attributed to the multipole–multipoleelectric interaction.⁴² In addition, the interaction strength can also be calculated using the following equation:⁴⁷

$$\frac{1}{x} = K \left\{ 1 + \beta(x)^{Q/3} \right\}^{-1} \tag{4}$$

where K and β are constants, I is emission intensity, and x is activator ion concentration. The dipole–dipole (d–d), dipole–quadruple (d–q), quadruple–quadruple (q–q) interactions take place with Q=6, 8, and 10, respectively. Fig. 10 shows the $\log(I/x)$ based on $\log(x)$ for the SrZrO₃:0.03Ho³⁺ phosphor. It can be observed that -Q/3=-2.24, so Q=6.72. Thus, the quenching in emission intensity of Ho³⁺ doped SrZrO₃ host lattices is due to dipole–dipole interactions. The concentration quenching of Ho³⁺ doped SrZrO₃ phosphor that occurred beyond the optimized concentration (3 mol%) is most useful for emitting green light in optoelectronic devices.

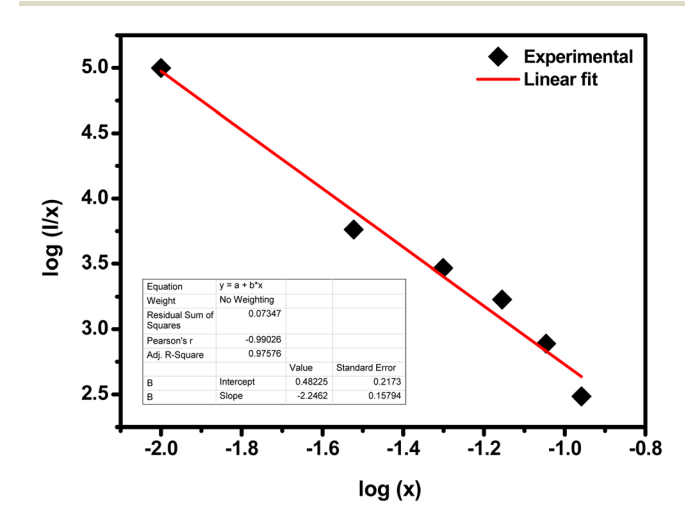


Fig. 10 Plot of $\log(I/x)$ as a function of $\log(x)$ of the $SrZrO_3:0.03Ho^{3+}$ phosphor (where I is the green emission peak intensity, and x is the Ho^{3+} ion concentration).

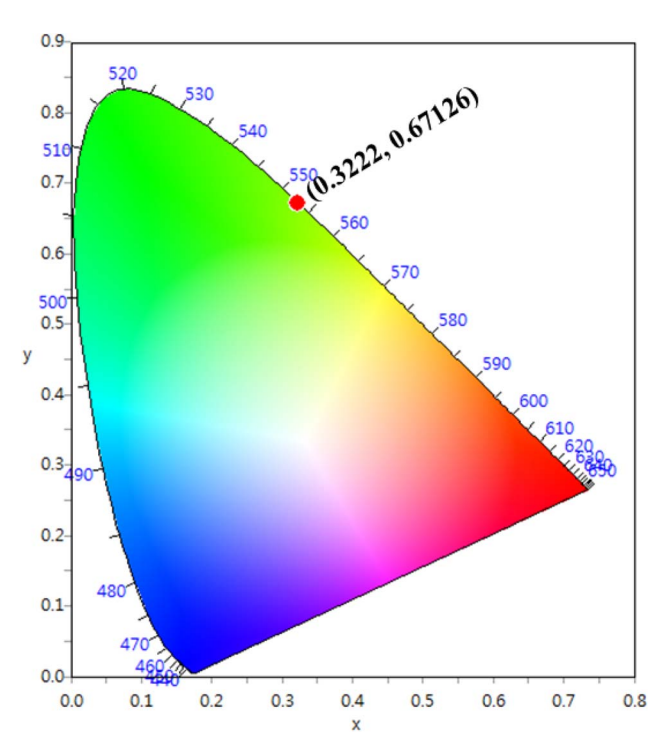


Fig. 11 CIE chromaticity diagram of SrZrO₃:0.03Ho³⁺ phosphor.

The CIE chromaticity coordinates were determined by the emission spectrum ($\lambda_{\rm exc} = 454 \text{ nm}$) of optimized Ho³⁺ (3 mol%) doped SrZrO₃ phosphor using 1931 CIE (Commission International de l'Eclairage France) technology, which is an accepted standard for the LED industry in matters related to colors, such as color mixing and color rendering. The chromaticity coordinates were found to be (0.322, 0.671) and this is situated in the green region of the CIE chromaticity diagram (see Fig. 11). The correlated color temperature (CCT) was also estimated by the McCamy experimental equation:48

$$CCT = -437n^3 + 3601n^2 - 6861n + 5514.31$$
 (5)

where $n = \frac{(x - x_e)}{(y - y_e)}$ with chromaticity epicenter being $x_e = 0.3320$ and $y_e = 0.1858$. The obtained CCT is 5654 K for the Ho³⁺ (3 mol%) doped SrZrO₃ phosphor. Thus, this could be useful for w-LEDs because a CCT < 5000 K gives warm-white LEDs for home gadgets.

3.5 Judd-Ofelt intensity parameters from PLE and radiative properties

The familiar Judd-Ofelt intensity parameters (Ω_{λ} with $\lambda = 2, 4$, and 6) were adopted to figure out the fluorescence branching ratios, spontaneous emission probabilities, and radiative lifetimes of the excited multiplets to assess the undertaking of lasers and luminescent materials. As per Judd-Ofelt (J-O) theory, ^{49,50} the J–O intensity parameters (Ω_{λ} with $\lambda = 2, 4$, and 6) can be examined conventionally from absorption spectra by evaluating the measured and computed spectral line strengths of the excited 4f-4f electronic transitions using least-square or chi-square fit methods. However, in recent decades, 42,51,52

ces	١	
<u>ن</u>	١	
Ħ	١	
ĭ		
یز	-	
ő	١	
7	ļ	
ns	١	
9	١	
var	١	
	١	
ped	١	
d	١	
Ō	١	
+ Μ.	١	
우	١	
_	١	
ō	١	
S	١	
Ĕ	١	
þ	١	
Ē	١	
.0	١	
ğ	١	
ō	١	
ã	١	
/a	-	
S	ļ	
Ĕ	- [
뱚	ļ	
X		
Θ		
eq	-	
Š	ļ	
ĕ	- [
ã	١	
0	١	
Je	١	
۲	١	
ç		
5	١	
CH		
0		
-2(
9	١	
X		
_		
Š	١	
S		
Ë	١	
ğ	١	
en	١	
šŧ	-	
a)	-	
.≧	-	
<u>-</u>		
.≥	-	
relat	-	
5	ļ	
9		
ō	- [
a	-	
4	- [
ζ,	-	
$\lambda = 2$	ļ	
\preceq		
<u>~</u>	-	
72	-	
\cong	ļ	
ts		
e	-	
Ē	ļ	
ĕ		
Α	-	
Ę.	-	
nai	ļ	
7	- [
eq	- [
Š	ļ	
ğ	ļ	
ā	-	
þ	-	
\sim		
⋾		
noo		
⋾		
noo		
Dou		
le 2 Dou		
ble 2 Dou		

					$^a\mathrm{SrZrO_3:0.03Ho^{3+}}$	03Ho ³⁺	$rac{ ext{YLiF}^{55}}{ ext{}}$	$GdLiF_4$ (ref. 55)	$\frac{\text{LuLiF}_4 \text{ (ref. 55)}}{}$
from $^5\mathrm{I_8} \rightarrow$	Excitation band wavenumber $(\nu \text{ cm}^{-1})$	$\ U^2\ ^2$	$\ U^2\ ^4$	$\ U^2\ ^6$	$S_{ m meas}^{ m ed}$	$S_{\mathrm{cal}}^{\mathrm{ed}}$	$S_{ m meas}^{ m ed}$	$S_{ m meas}^{ m ed}$	$S_{ m meas}^{ m ed}$
${}^{3}K_{6} + {}^{3}F_{4}$	29 922	0.0026	0.1263	0.0073	0.101	0.024	0.309	0.341	0.251
3 $_{19}$ + 5 $_{13}$	28 902	0.0185	0.0052	0.1169	0.080	0.031	0.394	0.379	0.300
${}^{3}\mathrm{H_{6}} + {}^{3}\mathrm{H_{5}}$	27 685	0.254	0.2337	0.1609	0.059	0.173	1.310	4.377	1.276
$^{5}G_{4} + ^{3}K_{7}$	25 846	0.0058	0.0361	0.0697	0.012	0.021	0.325	0.345	0.307
${}^{5}G_{5}$	23 872	0	0.5338	0.0002	0.087	0.085	1.161	1.199	1.120
${}^{5}G_{6}$	22 020	1.5201	0.8410	0.1535	0.809	0.791	3.893	4.177	4.014
$^{5}\mathrm{F}_{2} + {}^{3}\mathrm{K}_{8}$	21 186	0.0208	0.0334	0.3576	0.094	0.083	0.392	0.446	0.248
$^5\mathrm{F}_3$	20 542	0	0	0.3464	0.084	0.067	0.716	0.811	0.375
$\delta_{ m rms}$					0 #	± 0.011	\pm 0.117	\pm 0.114	$\pm \ 0.108$

a simple approach has been proposed to evaluate J–O intensity parameters from the assessment of excitation spectra. This approach is successfully applied to Nd^{3+} , Er^{3+} and Dy^{3+} doped various phosphor powders.

Normally, the excitation and absorption spectral difference lies in the intensity ratio of the fluorescence excitation to the absorption (i.e., relative fluorescence quantum efficiency). Therefore, the excitation and absorption spectra will coincide exactly while relative fluorescence quantum efficiency maintains to be constant at different wavelengths. Once the experimental excitation spectrum is corrected to the corresponding absorption spectrum in which the excited states are followed by a very fast non-radiative relaxation to the monitored level. 53,54 In this work, the excited multiplets of Ho³⁺: ⁵G₅, ⁵F₂(³K₈), ⁵G₆, ⁵F₃ levels are nonradiatively relaxed to ${}^5F_4 + {}^5S_2$ monitored level may satisfy the above statement, and excited multiplets chosen as ideal ones for the determination Judd-Ofelt parameters. The calculated and measured relative excited line strength for the attended electric-dipole transitions across the aJ and bJ' levels are determined using the following expressions,55,56

$$S_{\mathrm{cal}}^{\mathrm{ed}}(aJ;bJ') = \sum_{t=2,4,6} \mathcal{Q}_{\lambda} \left| \left\langle [\alpha SL]J \| U^{(\lambda)} \| [\alpha' S'L']J' \right\rangle \right|^{2}$$
 (6)

$$S_{\text{meas}}^{\text{ed}}(aJ;bJ') = \frac{3\text{ch}(2J+1)}{8\pi^3\overline{\lambda}e^2N_0} \frac{9n}{(n^2+2)^2} \Gamma_{\text{exc}}$$
 (7)

where Ω_{λ} is the J–O intensity parameter, which is used in the environmental field effect of intermixing states, *i.e.*, $4f^{N-1}5d$ and $4f^{N-1}5g$. $U(\lambda)$ is the doubly reduced matrix tensor operator and it is found in the coupling approximations approach, which is taken from the literature. The term $n \sim 2.12$ is the refractive index of SrZrO₃ material. The average wavelength of the excitation band is denoted as $\bar{\lambda}$, N_0 is the ion concentration and $\bar{\Lambda}$ is the integrated relative excitation intensity of each band. Ω_{λ} parameters were predicted by a least square fitting technique. Table 2 shows relative spectral line strengths of excited transitions for Ho³⁺ ions (3 mol%) in the SrZrO₃ phosphor. The root average square deviation $(\delta_{\rm rms})$ between experimental line strengths is,

$$\delta_{\rm rms} = \sqrt{\frac{\sum \left(S_{\rm exp}^{\rm ed} - S_{\rm meas}^{\rm ed}\right)^2}{(q - p)}} \tag{8}$$

where q and p are fitting parameters as transition number, and it has been used in our case as q=8 and p=3 in the best least square fitting procedure. The observed small $\delta_{\rm rms}$ value (see Table 2) is indicative of the validity and fit quality in J–O theory.

Table 3 describes the J–O intensity parameters considering various host matrices. The Ω_2 parameter indicates ionicity (or covalence) of RE-O bonds and is related to the local structure. Ω_4 and Ω_6 are non-sensitive to the dependence structure and are attributed to the stiffness of the host; however, the various active ions alter the characteristics of the evaluated spontaneous emission transitions. For example, from Table 3, the Ho³+ doped SrZrO₃ phosphor shows a lower ionic nature between Ho–O bonds compared with other oxide-based host

Table 3 Relative Judd–Ofelt intensity parameters, ($\Omega_{\lambda} \times 10^{-20} \text{ cm}^2$, $\lambda = 2$, 4 and 6) of various host matrices

Host	\mathcal{Q}_2	\mathcal{Q}_4	\mathcal{Q}_6	Order
^a SrZrO ₃ :0.03Ho ³⁺	0.41	0.16	0.19	$\Omega_{6} > \Omega_{4} > \Omega_{2}$ $\Omega_{4} > \Omega_{6} > \Omega_{2}$ $\Omega_{4} > \Omega_{6} > \Omega_{2}$ $\Omega_{4} > \Omega_{6} > \Omega_{2}$ $\Omega_{2} > \Omega_{4} > \Omega_{6}$
Y ₃ Al ₅ O ₁₅ (YAG) ⁵⁸	0.04	2.67	1.89	
Lu ₃ Al ₅ O ₁₂ (ref. 59)	0.17	2.08	1.92	
LaF ₃ (ref. 60)	1.16	1.38	0.88	
LiYF ₄ (ref. 61)	1.01	1.71	1.21	$\Omega_4 > \Omega_6 > \Omega_2$ $\Omega_4 > \Omega_6 > \Omega_2$ $\Omega_4 > \Omega_6 > \Omega_2$
LiYF ₄ (ref. 62)	0.96	2.05	1.43	
^a Present work.				

matrices. On the other hand, when compared with a fluoridebased host, the Ho^{3^+} doped SrZrO_3 phosphor shows a higher ionic nature between the Ho–O bonds because of the lesser values of the J–O intensity parameter, Ω_2 .

Conclusions

The SrZrO₃:Ho³⁺ phosphors were produced by a sol-gel system and were analyzed by X-ray diffraction, FTIR, UV-visible and photoluminescence spectroscopic techniques. We have identified absorption bands around 365, 421, 454, 468, 489, 542, and 645 nm from the UV-visible diffuse reflectance spectrum of the 4f-4f configuration of Ho3+ transitions. The optical band gaps $(E_{\rm opt})$ were found to be 5.21 eV (direct transition), 5.43 eV (indirect transition), respectively for the Ho3+ doped SrZrO3 phosphor. Upon 454 nm excitation, the Ho³⁺ doped SrZrO₃ phosphor exhibits high green and low red emission bands that are connected to the respective ${}^{5}F_{4} + {}^{5}S_{2} \rightarrow {}^{5}I_{8}$ (545 nm) and ${}^5F_5 \rightarrow {}^5I_8$ (652 nm) transitions of ${\rm Ho^{3^+}}$ ions. The fluorescence quenching of the studied phosphor samples was evaluated by looking at the critical distance between Ho-Ho ions as well as the strength of dipole-dipole (d-d), dipole-quadruple (d-q) and quadruple-quadruple (q-q) interactions. The obtained CCT was 5654 K for the optimum concentration of Ho³⁺ (3 mol%) doped in the SrZrO₃ phosphor suggesting that it may be useful for w-LEDs. In addition, using excitation spectrum of the optimized phosphor, the Judd-Ofelt intensity parameters (Ω_{λ} with $\lambda = 2, 4$ and 6) for Ho³⁺ were estimated and compared with other hosts. The observed results of photoluminescence properties suggested that the SrZrO₃:0.03Ho³⁺ phosphor may be advantageous for green emitting optoelectronic applications.

Conflicts of interest

There are no conflicts to declare.

Acknowledgements

This work was supported by the National Research Foundation of Korea (NRF) grant funded by the Korea government (MSIT) (2018M2B2A9065656). This paper was also supported by the KU Research Professor Program of Konkuk University.

RSC Advances References

- 1 S. K. Gupta, A. K. Yadav, D. Bhattachary, S. N. Jha and V. Natarajana, Visible light emitting Ln³⁺ ion (Ln=Sm, Eu and Dy) as a structural probe: A case study with SrZrO₃, *J. Lumin.*, 2015, **164**, 1–22.
- 2 K. Nonaka, M. Akiyama, C.-N. Xu, T. Hagio, M. Komatsu and A. Takase, Enhanced photovoltaic response in lead lanthanum zirconate-titanate ceramics with A-Site deficient composition for photostrictor application, *Jpn. J. Appl. Phys.*, 2000, **39**, 9A.
- 3 E. Caetano, C. Souza and R. Muccillo, Properties and applications of perovskite proton conductors, *Mater. Res.*, 2010, 13, 385–394.
- 4 M. Kubicek, A. H. Bork and J. L. M. Rupp, Perovskite oxides a review on a versatile material class for solar-to-fuel conversion processes, *J. Mater. Chem. A*, 2017, 5, 11983–12000.
- 5 M. Sukumar, L. John Kennedy, J. Judith Vijaya, B. Al-Najar, M. Bououdina and G. Mudhana, Structural, optical, and magnetic properties of Ca²⁺ doped La₂CuO₄ perovskite nanoparticles, *Vacuum*, 2019, 167, 407–415.
- 6 M. A. Peña and J. L. G. Fierro, Chemical structures and performance of perovskite oxides, *Chem. Rev.*, 2001, **101**, 1981–2018.
- 7 J. Etourneau, J. Portier and F. Ménil, The role of the inductive effect in solid state chemistry: how the chemist can use it to modify both the structural and the physical properties of the materials, *J. Alloys Compd.*, 1992, **188**, 1–7.
- 8 S. Katyayan and S. Agrawal, Study of optical behaviour of Eu³⁺ and Tb³⁺ doped zirconate perovskite phosphors prepared by molten salt technique, *Opt. Quantum Electron.*, 2020, **52**, 18.
- 9 N. R amadass, ABO₃-type oxides-Their structure and properties-a bird's eye view, *Mater. Sci. Eng.*, 1978, **36**, 231–239.
- 10 G. Pan, X. Bai, D. Yang, X. Chen, P. Jing, S. Qu, L. Zhang, D. Zhou, J. Zhu, W. Xu, B. Dong and H. Song, Doping lanthanide into perovskite nanocrystals: highly improved and expanded optical properties, *Nano Lett.*, 2017, 17, 8005–8011.
- 11 S. K. Gupta, P. S. Ghosh, A. K. Yadav, N. Pathak, A. Arya, S. N. Jha, D. Bhattacharyya and R. M. Kadam, Luminescence properties of SrZrO₃/Tb³⁺ perovskite: host-dopant energy-transfer dynamics and local structure of Tb³⁺, *Inorg. Chem.*, 2016, 554, 1728–1740.
- 12 S. K. Gupta, N. Pathak and R. M. Kadam, an efficient gelcombustion synthesis of visible light emitting barium zirconate perovskite nanoceramics: probing the photoluminescence of Sm³⁺ and Eu³⁺ doped BaZrO₃, *J. Lumin.*, 2016, **169**, 106–114.
- 13 S. K. Gupta, N. Pathak, R. Gupta, S. K. Thulasidas and V. Natarajan, Probing the oxidation state and coordination geometry of uranium ion in SrZrO₃ perovskite, *J. Mol. Struct.*, 2014, 1068, 204–209.
- 14 Z. Li, H. Duan, Y. Jin, S. Zhang, Y. Lv, Q. Xu and Y. Hu, Intrinsic defects and spectral characteristics of SrZrO₃ perovskite, *Phys. B*, 2018, **534**, 105–112.

- 15 K. S. Knight and C. L. Bulle, Low temperature and high pressure thermoelastic and crystallographic properties of SrZrO₃ perovskite in the Pbnm phase, *Solid State Sci.*, 2016, **62**, 90–104.
- 16 A. Mai, V. A. C. Haanappel, S. Uhlenbruck, F. Tietz and D. Stöver, Ferrite-based perovskites as cathode materials for anode-supported solid oxide fuel cells: Part I. variation of composition, *Solid State Ionics*, 2005, 176, 1341–1350.
- 17 E. Mete, R. Shaltaf and Ş. Ellialtıoğlu, Electronic and structural properties of a 4d perovskite: Cubic phase of SrZrO₃, *Phys. Rev. B: Condens. Matter Mater. Phys.*, 2003, **68**, 035119.
- 18 L. Bi, S. Boulfrad and E. Traversa, Steam electrolysis by solid oxide electrolysis cells (SOECs) with proton-conducting oxides, *Chem. Soc. Rev.*, 2014, 43, 8255–8270.
- 19 D. Souptel, G. Behr and A. M. Balbashov, SrZrO₃ single crystal growth by floating zone technique with radiation heating, *J. Cryst. Growth*, 2002, 236, 583–588.
- 20 C. J. Howard, K. S. Knight, B. J. Kennedy and E. H. Kisi, The structural phase transitions in strontium zirconate revisited, *J. Phys.: Condens. Matter*, 2000, **12**, 45.
- 21 R. E. A. McKnight, C. J. Howard and M. A. Carpenter, Elastic anomalies associated with transformation sequences in perovskites: I. Strontium zirconate, SrZrO₃, *J. Phys.: Condens. Matter*, 2000, **12**, L677–L683.
- 22 S. Yamanaka, K. Kurosaki, T. Oyama, H. Muta, M. Uno, T. Matsuda and S. -I. Kobayashi, Thermophysical properties of perovskite-type strontium cerate and zirconate, J. Am. Ceram. Soc., 2005, 88, 1496–1499.
- 23 L. Carlsson, High-temperature phase transitions in SrZrO₃, *Acta Crystallogr.*, 1967, 23, 901–905.
- 24 J. R. Sambrano, V. M. Longo, E. Longo and C. A. Taft, Electronic and structural properties of the (001) SrZrO₃ surface, *J. Mol. Struct.: THEOCHEM*, 2007, **813**, 49–56.
- 25 N. Singh, M. Seshadri, M. S. Pathak and V. Singh, Structural and photoluminescence properties of orange emitting perovskites SrZrO₃:Sm³⁺ phosphors for solid-state lighting, *Solid State Sci.*, 2019, **87**, 163–170.
- 26 R. Lisiecki, M. Głowacki, M. Berkowski and W. Ryba-Romanowski, Contribution of energy transfer processes to excitation and relaxation of Yb³⁺ ions in $Gd^+(Al,Ga)_5O_{12}:RE^{3+}$, Yb³⁺ ($RE^{3+}=Tm^{3+}$, Er^{3+} , Ho^{3+} , Pr^{3+}), *J. Lumin.*, 2019, 211, 54–61.
- 27 T. V. Gavrilović, D. J. Jovanović, K. Smits and M. D. Dramićanin, Multicolor upconversion luminescence of GdVO₄:Ln³⁺/Yb³⁺ (Ln³⁺ = Ho³⁺, Er³⁺, Tm³⁺, Ho³⁺/Er³⁺/Tm³⁺) nanorods, *Dyes Pigm.*, 2016, **126**, 1–7.
- 28 H. Huang, H. Zhou, J. Zhou, T. Wang, D. Huang, Y. Wu, L. Sun, G. Zhou, J. Zhana and J. Hu, Enhanced anti-stocks luminescence in LaNbO₄:Ln³⁺ (Ln³⁺ = Yb³⁺, Er³⁺/Ho³⁺/Tm³⁺) with abundant color, *RSC Adv.*, 2017, 7, 16777–16786.
- 29 S. K. Ranjan, A. K. Soni and V. K. Rai, Enhanced green upconversion emission in Ho³⁺:Gd₂O₃ phosphor by codoping of Yb³⁺ ions, Mater, *Mater. Today: Proc.*, 2017, 4, 5593–5598.

- 30 M. Zhongfei, H. Yihua and J. Guifang, Luminescence properties of Eu^{3+} and Ho^{3+} in Sr_2TiO_4 , *J. Rare Earths*, 2012, **30**, 744–747.
- 31 W. Shi, Z. Zhang, J. Qin, Y. Zhang, Y. Liu, Y. Liu, H. Gao and Y. Mao, Interface modification by up-conversion material of Ho³⁺-Yb³⁺-Li⁺ tri-doped TiO₂ to improve the performance of perovskite solar cells, *J. Alloys Compd.*, 2018, 754, 124–130.
- 32 P. Hou, B. Liu, Z. Guo, P. Zhou, B. Wang and L. Zhao, Effect of Ho doping on the crystal structure, surface morphology and magnetic property of BiFeO₃ thin films prepared via the sol-gel technology, *J. Alloys Compd.*, 2019, 775, 59–62.
- 33 S. Sharif, G. Murtaza, T. Meydan, P. I. Williams, J. Cuenca, S. H. Hashimdeen and F. Shaheen, Structural, surface morphology, dielectric and magnetic properties of holmium doped BiFeO3 thin films prepared by pulsed laser deposition, *Thin Solid Films*, 2018, 662, 83–89.
- 34 A. Hussain and B. Kumar, Intrinsic polarization and resistive leakage analyses in high performance piezo-/pyroelectric Ho-doped 0.64PMN-0.36PT binary ceramic, *Adv. Powder Technol.*, 2018, **29**, 3124–3137.
- 35 R. Wurm, O. Dernovsek and P. Greil, sol-gel derived $SrTiO_3$ and $SrZrO_3$ coatings on SiC and C-fibers, *J. Mater. Sci.*, 1999, 34, 4031–4037.
- 36 G. Venkatesh, B. Blessto, C. S. K. Rao, R. Subramanian and L. John Berchmans, Novel perovskite coating of strontium zirconate in Inconel substrate, *Mater. Sci. Eng.*, 2018, 314, 012010.
- 37 C.-Y. Liu and T.-Y. Tseng, Resistance switching properties of sol-gel derived SrZrO₃ based memory thin films, *J. Phys. D: Appl. Phys.*, 2007, **40**, 7.
- 38 A. Zhang, M. Lu, S. Wang, G. Zhou, S. Wang and Y. Zhou, Novel photoluminescence of SrZrO₃ nanocrystals synthesized through a facile combustion method, *J. Alloys Compd.*, 2007, 433, L7–L11.
- 39 C. Chen, W. Zhu, T. Yu, X. Chen, X. Yao and R. G. Krishnan, F. T.-I. R., structure and dielectric property investigation of strontium zirconate thin films prepared by MOD technique, *Surf. Coat. Technol.*, 2003, **167**, 245–248.
- 40 G. Cabello, L. Lillo, C. Caro, G. E. Buono-Core, B. Chornik, M. Flores, C. Carrasco and C. A. Rodriguez, Photochemical synthesis of AZrO₃-X thin films (A=Ba, Ca and Sr) and their characterization, *Ceram. Interfaces*, 2014, 40, 7761– 7768
- 41 V. B. Reddy and P. N. Mehrotra, Infrared and thermal studies of strontium zirconyl oxalate hexahydrate, *Thermochim. Acta*, 1979, **31**, 349.
- 42 C. Shivakumara, R. Saraf and P. Halappa, White luminescence in Dy³⁺ doped BiOCl phosphors and their Judd-Ofelt analysis, *Dyes Pigm.*, 2016, **126**, 154–164.
- 43 C. R. Kesavulu, H. J. Kim, S. W. Lee, J. Kaewkhao, N. Wantana, S. Kothan and S. Kaewjaeng, Optical spectroscopy and emission properties of Ho³⁺-doped gadolinium calcium silicoborate glasses for visible luminescent device applications, *J. Non-Cryst. Solids*, 2017, 474, 50–57.
- 44 L. Wang, B. K. Moon, S. H. Park, J. H. Kim, J. Shi, K. H. Kim and J. H. Jeong, Photoluminescence properties, crystal

- structure and electronic structure of a Sr₂CaWO₆:Sm³⁺ red phosphor, *RSC Adv.*, 2015, 5, 89290–89298.
- 45 G. Blasse, Energy transfer in oxidic phosphors, *Phys. Lett. A*, 1968, **28**, 444–445.
- 46 S. Das, S. Som, C. Y. Yang, S. Chavhan and C. H. Lu, Structural evaluations and temperature dependent photoluminescence characterizations of Eu³⁺ activated SrZrO₃ hollow spheres for luminescence thermometry applications, *Sci. Rep.*, 2016, **6**, 25787.
- 47 L. G. V. Uitert, Characterization of energy transfer interactions between rare earth ions, *J. Electrochem. Soc.*, 1967, **114**, 1048–1053.
- 48 X. C. S. McCamy, Correlated color temperature as an explicit function of chromaticity coordinates, *Color Res. Appl.*, 1992, 17, 142–144.
- 49 B. R. Judd, Optical absorption intensities of rare-earth Ions, *Phys. Rev.*, 1962, **127**, 750.
- 50 G. S. Ofelt, Intensities of crystal spectra of rare-earth ions, *J. Chem. Phys.*, 1962, 37, 511.
- 51 W. Luo, J. Liao, R. Li and X. Chen, Determination of Judd-Ofelt intensity parameters from the excitation spectra for rare-earth doped luminescent materials, *Phys. Chem.*, 2010, 12, 3276.
- 52 S. Dutta, S. Som and S. K. Sharma, Excitation spectra and luminescence decay analysis of K⁺ compensated Dy³⁺ doped CaMoO₄ phosphors, *RSC Adv.*, 2015, 5, 7380–7387.
- 53 X. Y. Chen, M. P. Jensen and G. K. Liu, Analysis of energy level structure and excited-state dynamics in a Sm³⁺ complex with soft-donor ligands: Sm(Et₂Dtc)₃(bipy), *J. Phys. Chem. B*, 2005, **109**, 13991.
- 54 X. Y. Chen, E. Ma and G. K. Liu, Energy levels and optical spectroscopy of Er³⁺ in Gd₂O₃ nanocrystals, *J. Phys. Chem. C*, 2007, **111**, 10404.
- 55 B. M. Walsh, G. W. Grew and N. P. Barnes, Energy levels and intensity parameters of Ho³⁺ ions in GdLiF₄, YLiF₄ and LuLiF₄, *J. Phys.: Condens. Matter*, 2005, **17**, 7643–7665.
- 56 W. T. Carnall, H. Crosswhite and H. M. Crosswhite, Energy level structure and transition probabilities in the spectra of the trivalent lanthanides in LaF3, *Argonne National Laboratory Report*, 1977.
- 57 R. D. Shannon, R. C. Shannon, O. Medenbach and R. X. Fischer, Refractive index and dispersion of fluorides and oxides, *J. Phys. Chem. Ref. Data*, 2002, **31**, 931–970.
- 58 M. Malinowski, Z. Frukacz, M. Szuflinskaa, A. Wnuk and M. Kaczkan, Optical transitions of Ho in YAG, *J. Alloys Compd.*, 2000, **300–301**, 389–394.
- 59 D. N. Patel, B. R. Reddy and S. K. Nash-Stevenson, Spectroscopic and two-photon upconversion studies of Ho³⁺-doped Lu₃Al₅O₁₂, *Opt. Mater.*, 1998, **10**, 225–234.
- 60 M. J. Weber, B. H. Matsinger, V. L. Dolan and G. Surratt, Optical transition probabilities for trivalent holmium in LaF₃ and YAlO₃, *J. Chem. Phys.*, 1972, 57, 562.
- 61 A. A. Kaminskii, Crystalline lasers: physical process and operating schemes, CRC, Florida, 1996.
- 62 C. Li, Y. Guyot, C. Linares, R. Moncorge and M. F. Joubert, Radiative transition probabilities of trivalent rare-earth ions in LiYF₄, *ASSL Proc*, 1993, **15**, 91.